RSC Advances

ROYAL SOCIETY OF CHEMISTRY

www.rsc.org/advances

RSC Advances

RSCPublishing

ARTICLE

Large d_{33} and Enhanced Ferroelectric/ Dielectric Properties of Poly(vinylidene fluoride)-based Composites Filled with $Pb(Zr_{0.52}Ti_{0.48})O_3$ Nanofibers

Jie Chang[1], Yang Shen*[1], Xiangcheng Chu*[1], Xuehui Zhang[1], Yu Song[2], Yuanhua Lin[1], Ce-Wen Nan[1] and Longtu Li[1]

$Pb(Zr_{0.52}Ti_{0.48})O_3$ (PZT) nanofibers with diameter of 150~200 nm are prepared via electrospinning and used as dielectric fillers in Poly(vinylidene fluoride) (PVDF)-based composite films. Highly flexible polymer composite films are fabricated with a solution cast method. Enhanced dielectric constants are obtained at low volume fraction of PZT nanofibers. The orientation of PZT nanofibers perpendicular to the external electric field gives rise to improved dielectric breakdown strength. A subsequent uniaxial stretching of the composite films leads to higher crystallinity and breakdown strength of the polymer composites, which is favorable for the polarization of the nanocomposites at higher electric fields. Enhanced ferroelectric properties, i.e., higher saturated and remnant polarization, are obtained in these composite films. High piezoelectric coefficient (d_{33}) of ~ 87.4 pm/V is also achieved for the polymer composite films filled with only 2.4 vol.% of PZT nanofibers. The results show that the PZT/PVDF composite films have potential applications in piezoelectric sensors, and even piezoelectric actuators

1 Introduction

Flexible polymer composite films are critical in a number of applications in the modern information and electronic industry[1]. Polymers with fine ferroelectric and piezoelectric properties, such as poly(vinylidene fluoride) (PVDF) and its co-polymers, have been studied as energy harvesting devices[2-5] and sensors[6]. With proper sample treatments a ferroelectric phase (β, which has an all-trans conformation) can be induced in these polymers[7-9]. However, pure polymers are limited by their low intrinsic dielectric constants (2–3), although their dielectric breakdown strength is rather high (> 300 kV/mm). On the other hand, ferroelectric ceramics and relaxor ferroelectrics such as $BaTiO_3$, $Pb(Mg_{1/3}\ Nb_{2/3})O_3$, $Pb(Zr_xTi_{1-x})O_3$ (PZT) exhibit high value of dielectric constant[10, 11]. But their brittleness and challenging processing conditions impede their use as embedded capacitors and high energy storage devices[12]. Over the past few decades, tremendous efforts have been devoted to the development of polymer/ceramic composites in the hope that both high dielectric constants and high breakdown strength could be obtained simultaneously[13-16]**.** In the 0–3 type polymer/ceramic composites in which zero-dimensional ceramic particles are introduced in a three-dimensional continuous polymer matrix, a very high concentration of ceramic particles is required (> 50 vol%) to induce high dielectric constants[17], which lead to poor mechanical properties of the composites and results in pores, voids or other structural defects. Subsequently, the dielectric breakdown strength of the polymer composites is also seriously compromised by these structural imperfections[18]. It is now commonly accepted that high dielectric constants must not achieved at the cost of decreased breakdown strength. The reasons are two folds: i) the static electrical energy density of the polymer composites is related to the dielectric constants (ε) and breakdown strength (E_b) as$1/2\varepsilon{E_b}^2$, where E_b plays a more important role than ε in determining the energy density of the polymer composites; ii) high breakdown strength also means that the polymer composites are highly insulating, which translates into lower leakage current and low dielectric loss. Plus, polymer composites with high breakdown strength could be polarized at higher electric field and thus exhibit enhanced ferroelectric or piezoelectric properties.

Recently, replacing spherical ceramic particles using fibers of large aspect ratio has been proved as an effective approach to increasing the dielectric constant of polymer composites at much lower volume fraction[19]. Their morphology also helps to reduce the surface energy[20], which prevents the nanofibers from aggregation in the polymer matrix. Surface modification of the ceramic fibers may further facilitate the homogeneous dispersion of the ceramic fibers in polymer matrix[21]. Moreover, surface modification also contributes to stronger interfaces between the ceramic fillers and the polymer matrices by forming interfacial bonds, which have a significant effect on the dielectric and piezoelectric properties[22]. In this contribution, $Pb(Zr_{0.52}Ti_{0.48})O_3$ nanofibers were prepared by electrospinning with their surface coated with dopamine layer and fused with

polyvinylidene fluoride (PVDF) into highly flexible composite films. Dopamine, which is a common biomaterial but has recently been used as a general building block for surface treatments of various materials, improves the compatibility between PZT nanofibers and the polymer matrix, leading to homogeneous dispersion of the fillers in the matrix[23]. Enhanced dielectric constants are obtained at low volume fraction of PZT nanofibers. The orientation of PZT nanofibers perpendicular to the external electric field gives rise to improved dielectric breakdown strength. A subsequent uniaxial stretching of the composite films leads to higher crystallinity and breakdown strength of the polymer composites, which is favorable for the polarization of the nanocomposites at higher electric fields[5]. Enhanced ferroelectric properties, i.e., higher saturated and remnant polarization, are obtained in these composite films. High piezoelectric coefficient (d_{33}) of ~ 87.4 pm/V is also achieved for the polymer composite films filled with only 2.4 vol.% of PZT nanofibers[24].

2 Experimental

2.1 Preparation of PZT nanofibers via electrospinning

All chemicals are purchased from Alfa Aesar and used with further purification. The preparation of PZT sol has been described in detail in previous contributions[26]. Briefly, for the preparation of lead and zirconium precursors, lead acetate trihydrate and zirconyl nitrate were dissolved in 2-methoxyethanol respectively by heating and stirring at 80 ^{o}C. Titanium precursor solution was then prepared by dissolving tetrabutyl titanate in 2-methoxyethanol, acetylacetone. The zirconium and titanium precursor solutions were mixed first and followed by the addition of lead precursor to form the PZT sol for electrospinning. The Zr/Ti molar ratio was kept 0.52 : 0.48, and 1 % more Pb was needed to compensate for the evaporation. To adjust the viscosity of the precursor sols, 0.5 g of polyvinyl pyrrolidone (PVP) was dissolved in 10 ml PZT solution.

During the electrospinning, the precursor solution was added in a syringe. The roller collector covered by aluminum foil was placed 15 cm from the tip of the syringe. A high voltage of 13 kV was applied during electrospinning. After electrospinning, the PZT_nfs textile was calcined at 600 ^{o}C for 3 h in a box furnace for the pyrolysis of the precursor sols. Differential scanning calorimetry (DSC, TGA/DSC1, Metter-Toledo, Switzerland) was used to identify the crucial steps in the pyrolysis and sintering processes, from room temperature to 900 ^{o}C, with a heating rate of 10°C/min. For surface treatment, the PZT nanofibers were then treated in the aqueous solution of dopamine hydrochloride (99.99%, Alfa Aesar) and stirred for 12 h at 60 ^{o}C, giving rise to amorphous layers of 2–3 nm formed uniformly on the surface of the PZT nanofibers.

The phase composition of the PZT nanofibers were characterized by scanning electron microscope (SEM, Hitachi S-4500) and X-ray powder diffraction (XRD, Bruke D8). The dopamine modified PZT nanofibers were characterized by fourier transform infrared spectroscopy (FTIR, Nicolet 6700) and high resolution transmission electron microscopy (HRTEM, JEOL2011).

2.2 Fabrication and characterization of the PZT/PVDF composite films

For the fabrication of the PZT/PVDF composites, the modified PZT nanofibers and PVDF were dispersed in N,N-dimethylformamide (DMF) by ultrasonication. Then the solution was casted to form PZT/PVDF composite films on glass substrates. After drying at 40 ^{o}C for 5 h, the composite films thus obtained were about 30-40 μm in thickness[27]. Copper electrodes of 4 mm diameter were deposited on both sides of the films for electrical measurements. For improved ferroelectric properties, the composite films were then subjected to uniaxial stretching by employing a universal tester (Shimadzu, AG-X) at a stretching rate of 10 mm/min at room temperature, with the stretch ratio of 4[5, 28]. The thickness of the stretched composite films were about 10~15 μm.

SEM, XRD and FTIR were performed for composites films. Meanwhile, dielectric properties were measured by employing a HP 4294 A precision impedance analyzer (Agilent Technologies) at room temperature. The electric breakdown strength was tested using a dielectric withstand voltage test (Beijing Electromechanical Research Institute Supesvoltage Technique) at a ramping rate of 200 V s^{-1} and a limiting current of 5 mA. Polarization–electric field (P–E) loops were measured by a Premier II ferroelectric test system (Radiant Technologies, Inc.). The bipolar strain-electric field (P-E) hysteresis loops were measured using a ferroelectric tester (aixACCT TF Analyzer 1000) at a fixed frequency of 1 Hz. A laser interferometer is coupled with TF 1000 for the measurement of strain.

3 Results and discussion

3.1 Characterization of PZT nanofibers

Figure S1 shows the thermogravimetric (TGA) curve and the corresponding differential thermal analysis (DTA) curve of the precursor solution. Below 200 ^{o}C, the weight loss shown in the TGA curve along with the weak broad endothermic DTA peak, is due to the evaporation of the volatile solvent. The sharp weight loss at 300 ^{o}C, which corresponds to a strong exothermic DTA peak, is due to the decomposition and removal of organic groups[29]. There is a weak exothermic peak in the DTA curve around 450 ^{o}C, indicating the start of the pervoskite phase formation.

The morphologies of PZT nanofibers are shown in figure 1 inset (a). The SEM image reveals that the uniform nanofibers are of large aspect ratio, i.e., diameters of 150–200 nm and lengths of tens of micrometers after calcination. The XRD patterns shown in figure 1 indicate that after the calcination at 600^{o}C the PZT nanofibers are well crystallized. The diffraction peak at around 44.8 ^{o} indicates that the real composition is close to the desired morphotropic phase boundary (MPB) –where the tetragonal and rhombohedral phases coexist and a maximum ferroelectric properties are expected[30].

After surface modification with dopamine, an amorphous layer is coated on the surface of the PZT nanofibers as shown in the HRTEM image in Figure 1 inset (b). A survey with TEM images indicates that the surface layers are uniform and of high structural integrity. The red highlight reveals that the layers are of 2–3 nm in thickness[31]. The uniform layers coated on the PZT nanofibers are further characterized by FTIR in the range of 400–4000 cm^{-1} as shown in Figure S2. The absorption bands at 1633, 1426, and 1084 cm^{-1} are related to N-H bending vibration, aromatic C-C stretching vibration and aromatic amine C-N stretching bands, respectively[24]. The results prove the existence of aromatic and amido groups of dopamine.

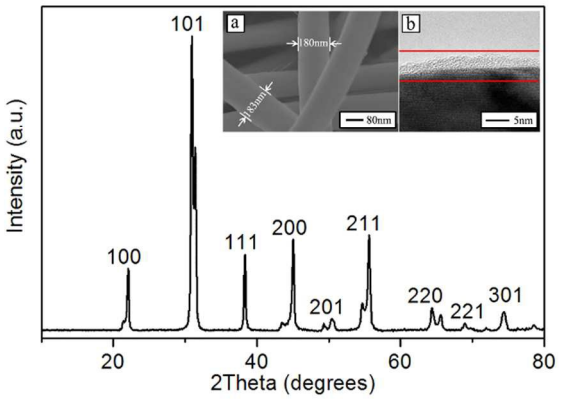

Fig. 1 X-ray diffraction pattern of PZT nanofibers after calcination. Insert (a) SEM images of calcined electrospinning nanofibers, (b) HRTEM image of the PZT nanofiber after surface modification by dopamine.

3.2 Morphology of PZT/PVDF composite films

Figure 2 shows typical surface SEM images of the PZT/PVDF composite filled with increasing amount of PZT nanofibers. Below 8.7 vol. %, homogeneous dispersions of PZT nanofibers in PVDF matrices could be achieved as a result of the better compatibility, as seen in Figure 2(a)–2(c). Further addition of PZT nanofibers leads to the formation of clusters of PZT nanofibers and voids on the surface, as shown in Figure 2(d)-2(e). Given the good microstructural integrity as well as the small loading of PZT nanofibers, superior flexibility is achieved even at the highest loading of the PZT nanofibers. Figure 2(f) shows the aligned nanofibers along the stretching direction.

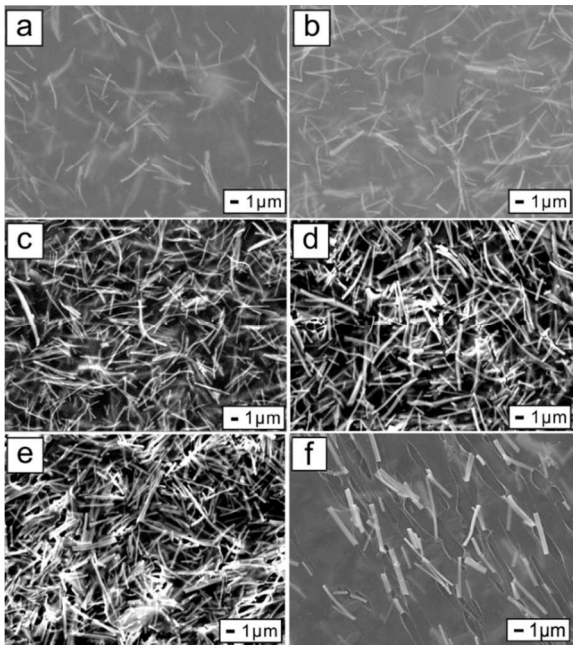

Fig. 2 Surface SEM images for PZT/PVDF composites filled with (a) 2.4 vol. %, (b) 5.2 vol. %, (c) 8.7 vol. %, (d) 12.9 vol. %, (e) 18.2 vol. % of PZT nanofibers and (f) 2.4 vol.% after stretching.

Figure 3 shows the XRD patterns of PZT/PVDF composite films with various volume ratios of PZT nanofibers. PVDF film mainly consists of α phase, and PZT phase plays a predominant role with the increasing volume ratio[9]. FTIR spectra of PVDF and PZT/PVDF composites in the range of 600–1600 cm^{-1} are shown in Figure 4. The bands at 614 and 764 cm^{-1} correspond to the α phase PVDF, while the bands at 840 and 1274 cm^{-1} are attributed to the β or γ phase of PVDF[29]. The strong absorption at 636 cm^{-1} of PZT/PVDF film may result from the Ti–O bond and perovskite phase[30].

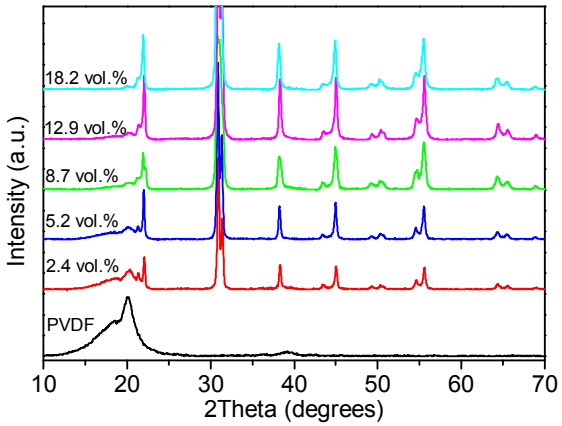

Fig. 3 X-ray diffraction patterns of PZT/PVDF composite films with increasing volume fraction of PZT nanofibers

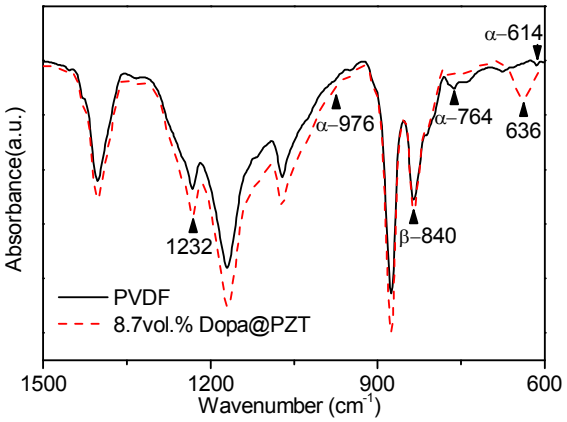

Fig. 4 The FT-IR of the PVDF films before (solid line) and after (dashed line) adding dopamine-modified PZT nanofibers

3.3 Dielectric properties of PZT/PVDF composites

Shown in Figure 5 are the frequency-dependent dielectric constant and the dielectric loss of the PZT/PVDF composite films. As seen, the dielectric constants of the composites gradually increases with increasing volume fraction of PZT nanofibers and reaches up to 32 at 18.2 vol.% PZT nanofibers. The polymer matrix is dominant in determining the dielectric behavior of the composites. The decrease in the dielectric constant of the composites with increasing frequency is attributed to the reduction of the dipolar contribution at high frequency[31], and the dielectric loss of the composites remains low at low frequency and shows a wide peak at high frequency as a result of the dielectric relaxation of the polymer matrix.

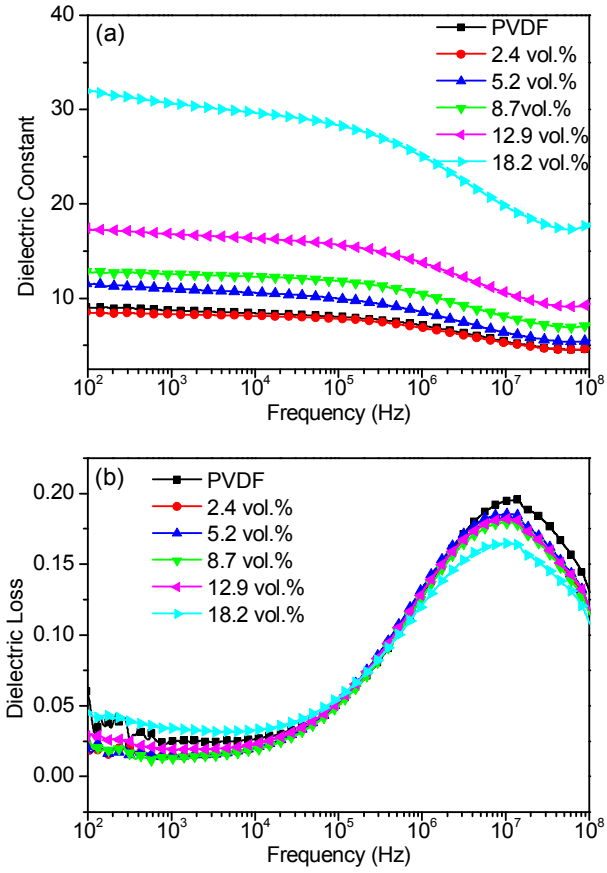

Fig. 5 Frequency-dependence of (a) dielectric constants and (b) dielectric loss for PZT/PVDF composites with different volume fractions of dopamine-modified PZT nanofibers

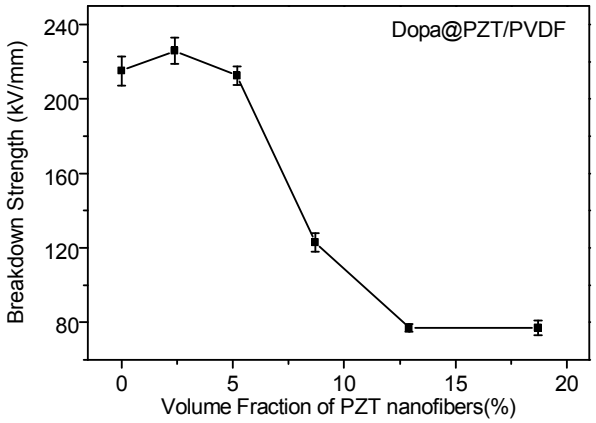

Fig. 6 Variations of the breakdown strength for the PZT/PVDF composite films with the dopamine-modified PZT nanofiber loading

The dependence of the breakdown strength on the volume fraction of PZT nanofibers are shown in Figure 6. The PVDF matrix has a breakdown strength (E_b) of (215±8) kV/mm. A small increase to (226±7) kV/mm is observed at 2.4 vol.%, then E_b begins to decrease with further addition of PZT nanofibers. This phenomenon that enhanced E_b at low loading of fillers followed by marked decrease in E_b upon further addition of dielectric fillers, has been observed by a number of researchers[32, 33]. When nanofillers are introduced in to the polymer matrix there is a change in the morphology of the polymer induced by the interaction of the polymer with the nanofiller. This may lead to the interfacial nanolayer around the nanoparticles, which will strengthen the interfaces in turn. A small amount of fillers are in favor of tightly bonding of the polymer chains to the fillers, which decreases the mobility of the polymer chains and leads to smaller probability of charge transferring during electric breakdown[32]. Recent research also indicates that surface modification of nanofibers by dopamine is capable of increasing E_b of polymer composites by over 100% as compared with pure polymer matrices[28]. Here in this case, the improved breakdown strength could also be attributed to the combined effects of surface modification and large aspect ratio of PZT nanofibers. The decrease of E_b at higher volume fractions of PZT nanofibers might be attributed to the voids present near the filler particles resulting in further field enhancement[34]. The combined effect of the surface discharges, the localized partial discharges at the particle sites can lead to the final breakdown of the polymer.

3.4 Ferroelectric and piezoelectric properties of PZT/PVDF composites

The P-E loops measured under 1 Hz of the as-prepared composite films are shown in Figure 7a. For the pristine PVDF, and nanocomposites with 2.4 vol.% and 5.2 vol.% of PZT nanofibers, the P-E loops are obtained under the similar saturated polarization electric field of ~ 200 kV/mm. As the breakdown strength decreases dramatically when the volume fraction of PZT nanofibers is larger than 8.7 vol.%, the maximum electric field applicable to the nanocomposites decreases substantially. Nevertheless, the P-E loops still provide insights of the polarization behavior of these nanocomposites. As seen, when the content of PZT nanofibers is < 5.2 vol.%, the maximum polarization of the composite films increases mildly from ~ 2.1 μC/cm^2 for the pristine PVDF to ~ 2.9 μC/cm^2 at 5.2 vol.% of PZT nanofibers. Further increase in the volume fraction of PZT nanofibers leads to substantial decrease in the breakdown strength of the composite films, as shown in Figure 6. As suggested by the shapes of these hysteresis loops, the observed electric polarization of the PZT/PVDF composite films may not be attributed to the switching of the ferroelectric domains, albeit the fact that both PVDF and PZT are ferroelectric in nature. Rather, the lossy P-E loops are indicative of space charge polarization. To improve the ferroelectric performance of the composite films, uniaxial stretching is applied to the composite films at room temperature. The benefits of stretching are two folds. First, the uniaxial stress applied is favorable for the transformation of PVDF into the ferroelectric β-polymorph, as indicated by the XRD patterns of the stretched pristine PVDF films (inset of Figure 7b). As an order-disorder type ferroelectric, the origin of ferroelectricity in polymer is rather different from that of inorganic ones. Thus, dipole orientation change is the most critical factor. The β-phase with all-trans bond (TTTT) conformation possess the highest net dipole moment among the four different polymorphs, which displays large piezoelectric and dielectric properties[38]. Plus, the oriented PZTnanofibers could also induce dipole orientation changes of the ferroelectric PVDF [39, 40]. Second, the deformation of the composite films during the stretching process eliminates the structural defects in the composite films and decrease the thickness of the composite films, which gives rise to enhanced breakdown strength and allows the films to be polarized to higher electric field[41]. All these favorable features synergistically lead to much improved

ferroelectric performance of these composite films. As shown in Figure 7b, a characteristic ferroelectric P-E loop, with a saturate polarization (P_s) of ~ 12 μC/cm^2 at ~ 220 kV/mm and remnant polarization (P_r) of ~ 7.5 μC/cm^2, is observed for the stretched pristine PVDF film. The introduction of only 2.4 vol. % of PZT nanofiber in the stretched PVDF films increases the breakdown strength of the composite film up to ~ 300 kV/mm. Although very mild increase in P_s and P_r is observed for the stretched PZT/PVDF composite films, the coercive field (E_c) increases substantially from ~ 50 kV/mm for pristine PVDF to ~ 100 kV/mm for the PZT/PVDF composite films.

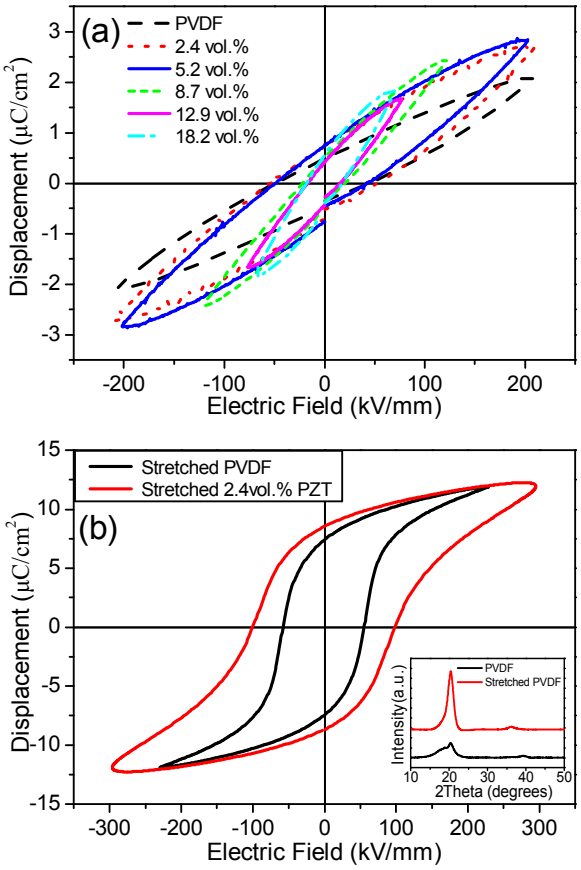

Fig. 7 room temperature P–E loops for (a) PVDF-based composites filled with different volume fraction of dopamine-modified PZT nanofibers before stretching and (b) composites with 2.4 vol.% of PZT nanofibers and pristine PVDF films after stretching. The improved crystallinity of the stretched-PVDF could be better distinguished in the XRD patters shown in the inset of (b).

The room temperature stretching process also has substantial effects on the piezoelectric performance of these composite films. As shown in the bipolar strain-electric field loops (Figure 8), a maximum strain of ~ 0.1% is observed for the as-prepared PVDF film at ~ 150 kV/mm, which translates into a d_{33} of ~ 6.6 pm/V. A much higher strain of ~ 1.1 % is then obtained in the stretched PVDF film at ~ 220 kV/mm, i.e., d_{33} of ~ 44 pm/V. Adding 2.4 vol.% of the piezoelectric PZT nanofibers enhances the strains even further up to ~ 2.6% at ~ 295 kV/mm. A remarkably high d_{33} of ~ 87.4 pm/V is achieved in the PZT/PVDF composite films. Same enhancement of piezoelectric coefficients has also been observed in a PVDF/magnetite nanocomposites. The introduction of 2 wt.% of magnetite nanoparticles gives rise to an enhancement of d33 by 5 magnitudes over the pristine PVDF. Such change of piezoelectric response is attributed to the relative long arrangement of PVDF units along the direction of electric field under high electric field[36].

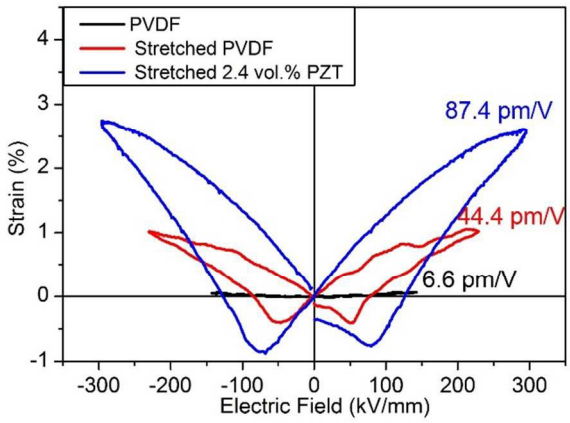

Fig. 8 Bipolar Strain-Electric Field loops for composites with 2.4 vol.% of PZT nanofibers and pristine PVDF films before/after stretching. Also superimposed are the d33 determined from the corresponding composite films.

Conclusions

PZT nanofibers have been prepared via electrospinning and were modified with the dopamine. Flexible PVDF-based composite films are prepared via solution-cast method. Enhanced dielectric constants are obtained at low volume fraction of PZT nanofibers. The orientation of PZT nanofibers perpendicular to the external electric field gives rise to improved dielectric breakdown strength. The uniaxial stretching of the composite films leads to higher crystallinity and breakdown strength of the polymer composites, which is favorable for the polarization of the nanocomposites at higher electric fields. Enhanced ferroelectric properties, i.e., higher saturated and remnant polarization, are obtained in these composite films. High piezoelectric coefficient (d_{33}) of ~ 87.4 pm/V is also achieved for the polymer composite films filled with only 2.4 vol.% of PZT nanofibers. The results show potential applications in piezoelectric sensors or even actuators.

Acknowledgements

This work was supported by the the National Basic Research Program of China (Grant No. 2015CB654604), NSF of China (Grant Nos. 51222204 & 51221291), Beijing Nova Program (Grant No.: XX2013037) and Tsinghua University (Grant No.20121087925 & 20131089218)

Notes and references

1 State Key Laboratory of New Ceramics and Fine Processing, School of Materials Science and Engineering, Tsinghua University, Beijing, 100084, P. R. China. Tel.: +86 10 62794855; Fax: +86 10 62772507; E-mail: shyang_mse@tsinghua.edu.cn; chuxiangcheng@tsinghua.edu.cn;

2 Laboratory of Advanced Energy Storage Materials & Devices, Research Institute of Tsinghua University in Shenzhen, Shenzhen, 518057, China

1 Z. M. Dang, J. K. Yuan, S. H. Yao and R. J. Liao, Adv Mater, 2013,

25, 6334-6365.
2 L. K. Wu, W. F. Yuan, T. Nakamura, S. Atobe, N. Hu, H. Fukunaga, C. Chang, Y. Zemba, Y. Li, T. Watanabe, Y. L. Liu, Alamusi, H. M. Ning, J. H. Li, H. Cui and Y. J. Zhang, Adv Compos Mater, 2013, 22, 49-63.
3 Y. Wang, X. Zhou, Q. Chen, B. Chu and Q. Zhang, Ieee T Dielect El In, 2010, 17, 1036-1042.
4 L. Zhu, J Phys Chem Lett, 2014, 5, 3677-3687.
5 W. Li, Q. Meng, Y. Zheng, Z. Zhang, W. Xia and Z. Xu, Appl Phys Lett, 2010, 96.
6 H. Luo and S. Hanagud, J Aerospace Eng, 1999, 12, 21-28.
7 Q. M. Zhang, V. Bharti and X. Zhao, Science, 1998, 280, 2101-2104.
8 D. Guo, F. Zeng and B. Dkhil, J Nanosci Nanotechno, 2014, 14, 2086-2100.
9 D. Guo, X. Chen, X. Chu, F. Zeng, Y. Bai, J. Cao and B. Dkhil, J Appl Phys, 2013, 113.
10 Z. Y. Cheng, R. S. Katiyar, X. Yao and A. S. Bhalla, Phys Rev B, 1998, 57, 8166-8177.
11 K. Yu, H. Wang, Y. Zhou, Y. Bai and Y. Niu, J Appl Phys, 2013, 113.
12 A. Srivastava, P. Maiti, D. Kumar and O. Parkash, Compos Sci Technol, 2014, 93, 83-89.
13 J. Nunes-Pereira, V. Sencadas, V. Correia, J. G. Rocha and S. Lanceros-Mendez, Sensor Actuat A-Phys, 2013, 196, 55-62.
14 Y. Rao, S. Ogitani, P. Kohl and C. P. Wong, J Appl Polym Sci, 2002, 83, 1084-1090.
15 Y. Bai, Z. Y. Cheng, V. Bharti, H. S. Xu and Q. M. Zhang, Appl Phys Lett, 2000, 76, 3804-3806.
16 P. Mishra and P. Kumar, Compos Sci Technol, 2013, 88, 26-32.
17 M. T. Sebastian and H. Jantunen, Int J Appl Ceram Tec, 2010, 7, 415-434.
18 K. Arlt and M. Wegener, Ieee T Dielect El In, 2010, 17, 1178-1184.
19 N. Guo, S. A. DiBenedetto, P. Tewari, M. T. Lanagan, M. A. Ratner and T. J. Marks, Chem Mater, 2010, 22, 1567-1578.
20 V. Tomer, G. Polizos, C. A. Randall and E. Manias, J Appl Phys, 2011, 109.
21 H. M. Jung, J. H. Kang, S. Y. Yang, J. C. Won and Y. S. Kim, Chem Mater, 2010, 22, 450-456.
22 Y. Song, Y. Shen, H. Y. Liu, Y. H. Lin, M. Li and C. W. Nan, J Mater Chem, 2012, 22, 16491-16498.
23 C. E. Chang, V. H. Tran, J. B. Wang, Y. K. Fuh and L. W. Lin, Nano Lett, 2010, 10, 726-731.
24 J. Wang, Z. Li, Y. Shen, Y. H. Lin and C. W. Nan, J Mater Sci, 2013, 48, 1021-1026.
25 Y. Song, Y. Shen, P. H. Hu, Y. H. Lin, M. Li and C. W. Nan, Appl Phys Lett, 2012, 101.
26 B. Mohammadi, A. A. Yousefi and S. M. Bellah, Polym Test, 2007, 26, 42-50.
27 Y. Wang and J. J. Santiago-Aviles, Integr Ferroelectr, 2011, 126, 60-76.
28 J. Heiber, A. Belloli, P. Ermanni and F. Clemens, J Intel Mat Syst Str, 2009, 20, 379-385.
29 P. H. Hu, Y. Song, H. Y. Liu, Y. Shen, Y. H. Lin and C. W. Nan, J Mater Chem A, 2013, 1, 1688-1693.
30 Y. Song, Y. Shen, H. Y. Liu, Y. H. Lin, M. Li and C. W. Nan, J Mater Chem, 2012, 22, 8063-8068.
31 D. Guo, S. Ikeda and K. Saiki, J Phys-Condens Mat, 2010, 22.
32 L. Yu and P. Cebe, Polymer, 2009, 50, 2133-2141.
33 M. Zhang, X. D. Wang, F. M. Wang, I. Salvado, P. M. Vilarinho and W. C. Li, Ceram Int, 2005, 31, 281-286.
34 Y. Y. Lu, J. Claude, L. E. Norena-Franco and Q. Wang, J Phys Chem B, 2008, 112, 10411-10416.
35 M. G. Danikas and T. Tanaka, Ieee Electr Insul M, 2009, 25, 19-25.
36 P. Preetha and M. J. Thomas, Ieee T Dielect El In, 2011, 18, 1526-1534.
37 R. Lovell, Electrical Insulation, IEEE Transactions on, 1976, EI-11, 110-114.
38 H. Ye, L. Yang, W. Shao, S. Sun and L. Zhen, RSC Advances, 2013, 3, 23730-23736.
39 D. Guo and N. Setter, Macromolecules, 2013, 46, 1883-1889.
40 D. Guo, I. Stolichnov and N. Setter, J Phys Chem B, 2011, 115, 13455-13466.
41 D. L. Chinaglia, Jr. R. Gregorio and D. R. Vollet, J Appl Polym Sci, 2012, 125, 527-535.
42 Z. Ouyang, E. Chen and T. Wu, J Appl Polym Sci, 2014, 131.